Ab initio study of van der Waals interaction of CO_2 with Ar

Peter J. Marshall and M. M. Szczęśniak
Department of Chemistry, Oakland University, Rochester, Michigan 48309

Joanna Sadlej and Grzegorz Chałasiński
Department of Chemistry, University of Warsaw, Pasteura 1, 02-093 Warszawa, Poland

Marc A. ter Horst
Department of Chemistry, Northwestern University, Evanston, Illinois 60208

Cynthia J. Jameson
Department of Chemistry M/C 111, University of Illinois at Chicago, Chicago, Illinois 60607

(Received 13 November 1995; accepted 29 January 1996)

The *ab initio* potential energy surface of the $ArCO_2$ cluster is calculated using the supermolecular Møller–Plesset perturbation theory (S-MPPT) and dissected into its fundamental components; electrostatic, exchange, induction, and dispersion energies. The surface contains a single minimum for the perpendicular approach of Ar toward the C atom which has a well depth of ~ 210 cm^{-1} at $R=6.5\ a_0$. This value is obtained using an extended basis set supplied with the bond functions and the fourth order supermolecular Møller–Plesset calculations, and is expected to be accurate to within $\pm 5\%$. The areas of the surface corresponding to the collinear approach of Ar to CO_2 contain an extended plateau. The saddle point in this region for $R=9.0\ a_0$ is stabilized by 117 cm^{-1}. The analytical pair potential for Ar–CO_2 obtained by fitting to the individual interaction components is provided. The three-body effects in the related cluster, Ar_2CO_2, are examined for two configurations of the Ar_2CO_2 cluster. The overall nonadditivity is dominated by the three-body dispersion effect; however, the exchange nonadditivity is the most anisotropic. The sources of this anisotropy are discussed. [S0021-9606(96)02217-6]

I. INTRODUCTION

The collisions of the CO_2 molecule with other atmospheric gases are of great importance to studies of atmospheric phenomena. The dynamics of these collisions can be investigated via the experimental measurements and theoretical predictions of collision-induced line shapes. As shown recently by Green and Hutson for Ar–HF the pressure-broadened line shapes can be accurately predicted using the potential energy surfaces obtained from van der Waals spectroscopy.[1] However, no such a potential energy surface exists even for the interaction of CO_2 with Ar, one of the simplest model system involving CO_2.

Due to the importance of the $ArCO_2$ interaction for atmospheric modeling, several semiempirical potential energy surfaces (PESs) have been proposed in the last two decades. The earliest family of semiempirical PESs for $ArCO_2$ was obtained by Parker, Snow, and Pack[2] and by Preston and Pack[3] on the basis of electron-gas calculations and fits to the second virial coefficients of CO_2+Ar. The first spectroscopic data on this complex were provided by Klemperer *et al.*[4] using the microwave spectroscopy. These studies determined that the equilibrium structure is T-shaped. The microwave results were used by Hough and Howard to construct the next generation of empirical PESs.[5] $ArCO_2$ has also been studied by infrared spectroscopy.[6,7] These data have been incorporated in the latest refinement of empirical PESs for this system by Bohac *et al.*[7] The quality of these surfaces was evaluated in a recent study by Roche *et al.*[8] which examined the ability of these empirical surfaces to reproduce both the high-resolution spectroscopic data for $ArCO_2$ and the pressure-broadening data. They concluded that these PESs did not correctly reproduce the shape of the repulsive wall of the PES. Such a wall can be most reliably obtained from *ab initio* calculations.

To the best of our knowledge the task of evaluating the Ar–CO_2 PES from the first principles has not yet been undertaken. In this paper we describe an *ab initio* study of the Ar–CO_2 interaction by means of combination of intermolecular and supermolecular Møller–Plesset perturbation theory (S-MPPT).[19–16]

II. METHOD AND DEFINITIONS

The supermolecular Møller–Plesset perturbation theory (S-MPPT) interaction energy corrections are derived as the difference between the values for the total energy of the dimer and the sum of the subsystem energies, in every order of perturbation theory

$$\Delta E^{(n)}=E_{AB}^{(n)}-E_A^{(n)}-E_B^{(n)} \quad n=\mathrm{SCF},2,3,4,\ldots\ . \tag{1}$$

Each individual $\Delta E^{(n)}$ correction can be interpreted[12–16] in terms of intermolecular Møller–Plesset Perturbation Theory (I-MPPT) which encompasses all well defined and meaningful contributions to the interaction energy such as electrostatic, induction, dispersion, and exchange, and may be expressed in the form of a double perturbation expansion.[9–11] The I-MPPT interaction energy corrections are denoted $\epsilon^{(ij)}$, where i and j refer to the order of the

intermolecular interaction operator and the intramolecular correlation operator, respectively (see Ref. 11 for more details).

A. Partitioning of ΔE^{SCF}

ΔE^{SCF} can be dissected as follows (cf. Refs. 12, 17, 18 for more details):

$$\Delta E^{\mathrm{SCF}}=\Delta E^{\mathrm{HL}}+\Delta E_{\mathrm{def}}^{\mathrm{SCF}}, \tag{2}$$

$$\Delta E^{\mathrm{HL}}=\epsilon_{\mathrm{es}}^{(10)}+\epsilon_{\mathrm{exch}}^{\mathrm{HL}}, \tag{3}$$

where ΔE^{HL} and $\Delta E_{\mathrm{def}}^{\mathrm{SCF}}$ are the Heitler–London and SCF-deformation contributions, respectively. ΔE^{HL} is further divided into the electrostatic, $\epsilon_{\mathrm{es}}^{(10)}$, and exchange, $\epsilon_{\mathrm{exch}}^{\mathrm{HL}}$, components. The SCF deformation originates from mutual electric polarization restrained by the Pauli principle (quantum exchange effects).[19] In this sense, the SCF deformation energy may be considered as a *quantum induction effect*. Two exchangeless approximations to $\Delta E_{\mathrm{def}}^{\mathrm{SCF}}$ are customarily considered, which are $\epsilon_{\mathrm{ind}}^{(20)}$ and $\epsilon_{\mathrm{ind},r}^{(20)}$, and may be viewed as two representations of the *classic induction effect*. The former describes the second-order induction effect at the uncoupled Hartree–Fock (UCHF) level, and the latter at the coupled Hartree–Fock (CHF) level (r denotes inclusion of response effects).[20]

Of all terms in Eqs. (2)–(3), only the electrostatic energy is additive whereas the HL-exchange and SCF-deformation parts give rise to many-body terms.

B. Partitioning of correlation terms

$$\Delta E^{(2)}=\epsilon_{\mathrm{es},r}^{(12)}+\epsilon_{\mathrm{disp}}^{(20)}+\Delta E_{\mathrm{def}}^{(2)}+\Delta E_{\mathrm{exch}}^{(2)}, \tag{4}$$

$\epsilon_{\mathrm{es},r}^{(12)}$ denotes the second-order electrostatic correlation energy with response effects[13,21] and $\epsilon_{\mathrm{disp}}^{(20)}$ the second-order Hartree–Fock dispersion energy. $\Delta E_{\mathrm{def}}^{(2)}$ and $\Delta E_{\mathrm{exch}}^{(2)}$ stand for the second-order deformation correlation correction to the SCF deformation and the second-order exchange correlation, respectively. The latter encompasses the exchange-correlation effects related to electrostatic correlation and dispersion and can be approximated as follows (provided the deformation-correlation contribution is negligible).[16]

$$\Delta E_{\mathrm{exch}}^{(2)}\cong\Delta E^{(2)}-\epsilon_{\mathrm{disp}}^{(20)}-\epsilon_{\mathrm{es},r}^{(12)}. \tag{5}$$

Since electrostatic and dispersion terms in Eq. (4) are additive, the only three-body terms arise in $\Delta E_{\mathrm{exch}}^{(2)}$ [and within $\Delta E_{\mathrm{def}}^{(2)}$ when it is not negligible].

The lowest order dispersion nonadditivity appears in the third order correction, $\Delta E^{(3)}$, as the $\epsilon_{\mathrm{disp}}^{(30)}$ correction which is related to the well-known Axilrod–Teller[22] nonadditivity. The $\epsilon_{\mathrm{disp}}^{(30)}$ term usually dominates $\Delta E^{(3)}$. More details on the many-body effects have been provided in Refs. 16, 23–25.

C. Calculations of interaction energies

Calculations of all the supermolecular ΔE values and perturbational interaction terms $\epsilon^{(ij)}$ are performed using the basis set of the entire complex.[26,27] With reference to supermolecular quantities this procedure amounts to applying the counterpoise method of Boys and Bernardi.[28] To assure the consistency of evaluation of the S-MPPT and I-MPPT interaction energy corrections, all the intermolecular perturbation terms, $\epsilon^{(ij)}$, must be derived in the basis set of the entire complex as well.

D. Geometries and basis sets

All calculations were carried out using the GAUSSIAN 92 program[29] and the intermolecular theory package written by Cybulski.[30]

The Jacobi coordinates R and Θ have been used for the Ar–CO_2 complex. R denotes the distance between the center of mass of the CO_2 molecule (which coincides with the C nucleus), and Θ corresponds to the angle between the R vector and the CO_2 axis. The interatomic separation C–O was set equal to 1.1612 Å.

The following basis sets were used in this work:

(1) For C and O, the medium-sized polarized basis set of Sadlej[31] $(10s,6p,4d/6s,4p)$ contracted to $[5s,3p,2d/3s,2p]$. For Ar, $(14s,7p,2d)$ contracted to $[7s,4p,2d]$ from Ref. 32. This selection has been termed S.
(2) The S basis set augmented with one set of f orbitals at each heavy atom; Ar ($\alpha_f=0.23$), O ($\alpha_f=0.18$), and C ($\alpha_f=0.258$). This basis set was termed Sdf.
(3) The Sdf basis set supplemented with a set of bond functions placed in the middle of the van der Waals bond. This basis set has been denoted $Sdf(b\text{-ext})$ and included the $[3s,3p,2d]$ set of Tao and Pan (sp exponents, 0.9, 0.3, 0.1; d exponents, 0.6, 0.2) from Refs. 33.

III. RESULTS AND DISCUSSION

The calculations of the PES were carried out for a full range of Θ and for the intermolecular distance R ranging from 5.0 a_0 to 10.0 a_0. The results obtained with the Sdf basis are listed in Table I, and angular scans at different R are illustrated in Fig. 1.

A. Characterization of the PES

For the PES obtained at the MP2/Sdf level the global minimum occurs at $R=7.0$ a_0 for the exactly T-shaped geometry, $\Theta=90°$. The related well-depth D_e amounts to 721.3 μE_{h}. The linear configurations at $R=9.0$ a_0 and $\Theta=0°$ and 180° is stabilized by 453.3 μE_{h} at the MP2/Sdf level. As seen in Table I at the MP2/Sdf level there exists a tiny ''barrier'' of 4 μE_{h} separating the linear configuration from the global minimum. However, this ''barrier'' is too small to be significant, and it disappears at the MP4/Sdf level (see Table I, entries in parentheses). Overall, in the region of R from 8.0 a_0 to 9.0 a_0 and for Θ from 0° to 60° the surface is extremely flat with no evidence of a distinct barrier.

To obtain better estimates of interaction energies of both configurations we performed MP4 calculations with the $Sdf(b\text{-ext})$ basis set for the T-shaped and collinear forms, and for various R, cf. Table II. The MP4 values of the interaction energies in Table II are our most accurate results. For the global minimum the related R_e and D_e were found to be

TABLE I. Angular dependence of the Ar–CO_2 interaction energy for different R calculated at the MP2/Sdf level. The values in parentheses correspond to MP4/Sdf calculations. Energy in μh and R in a.u.

$\Theta\backslash R$	5.0	6.0	7.0	8.0	8.5	9.0	9.5	10.0
0.0	463 790.00	74 330.00	8 526.30	116.93	−409.11	−453.25	−372.42	−279.63
					(−443.91)	(−482.56)	(−394.27)	
20.0	309 490.00	49 655.00	5 433.29	−150.47	−449.72	−432.49	−342.23	−253.91
					(−485.10)	(−460.35)	(−362.35)	
40.0	113 720.00	16 961.00	1 269.50	−444.82	−444.64	−358.11		−195.95
				(−496.29)	(−475.44)			
60.0	31 801.00	3 445.50	−352.60	−467.30		−269.12		−142.96
80.0	9 826.10	−28.66	−695.79	−419.28		−217.85		−115.06
90.0	7 806.40	−339.02	−721.27	−411.28		−211.40		−111.62
			(−757.5)					

6.5 a_0 and 957 μE_h, respectively, and for the linear form the stabilization of 532 μE_h was found for $R=9.0$ a_0.

B. Interaction energy partitioning and sources of anisotropy

The interaction energy perturbation components calculated with the Sdf basis set are reported in Table III and plotted in Figs. 2 and 3 for $R=7.0$ a_0. The HL-exchange term (Table III and Fig. 2) displays a strong angular dependence with a minimum at 90° and maxima at 0° and 180°. A wide niche of the HL-exchange plot at 60°–120° suggests depletion of the electron density around the central C atom. The existence of the niche around the C atom was confirmed by the plots of Laplacian of charge density of Bader and Keith[34] which showed a distinct depletion of electron density in this area (see their Fig. 1). Towards the O atoms the HL-exchange rapidly rises (beginning at 40°). Part of this rising may be attributed to the choice of the R coordinate that for 0° makes O lie in-between C and Ar. Nevertheless, the data in Table III and the plot in Fig. 2 as well as additional calculations with R fixed at the center of mass of the CO fragment (not reported) led to a conclusion that no additional features of electron density, such as depletions or concentrations, appear at the outskirts of the terminal O atoms. In particular, there is no evidence of the lone pairs at the O atoms. This is again in accord with the plots of Laplacian of charge density of Bader and Keith.[34]

The anisotropies of $\epsilon_{es}^{(10)}$, ΔE_{def}^{SCF}, and $\epsilon_{ind,r}^{(20)}$ are quite similar and qualitatively reciprocal to the anisotropy of the HL-exchange, see Fig. 3. $\epsilon_{ind,r}^{(20)}$ represents a poor quantitative approximation to ΔE_{def}^{SCF} in particular when close to O atoms, a typical feature of complexes with Ar. Interestingly, $\epsilon_{es}^{(10)}$ appears to be very similar to ΔE_{def}^{SCF}.

The correlation components are plotted in Fig. 3. As usual, $\Delta E^{(2)}$ is dominated by the dispersion terms $\epsilon_{disp}^{(20)}$. $\epsilon_{es,r}^{(12)}$ is practically negligible. $\Delta E_{exch}^{(2)}$ is small but not negligible in the region of terminal O atoms. For large R (see Table III) the shape of PES is determined by the dispersion component. For small R the shape is determined by the HL-exchange component.

For the purposes of semiempirical modeling of the PES of $ArCO_2$ it is of primary importance to examine a model which is often used in such studies, namely SCF+DISP. The SCF+DISP surface was constructed as sum of the ΔE^{SCF} and $\epsilon_{disp}^{(20)}$ terms evaluated using the Sdf basis set (see Table III), and is shown in Fig. 4. By comparison with the MP2 surface (see Fig. 1) the SCF+DISP PES is too low in energy which is a familiar feature of this model.[16] Its global minimum shifts to too-short distances, $R=6.0$ a_0. However, the basic shape remains nearly the same, namely, the SCF +DISP surface contains a very flat plateau for geometries close to linear with no barrier between the global minimum and the linear structure.

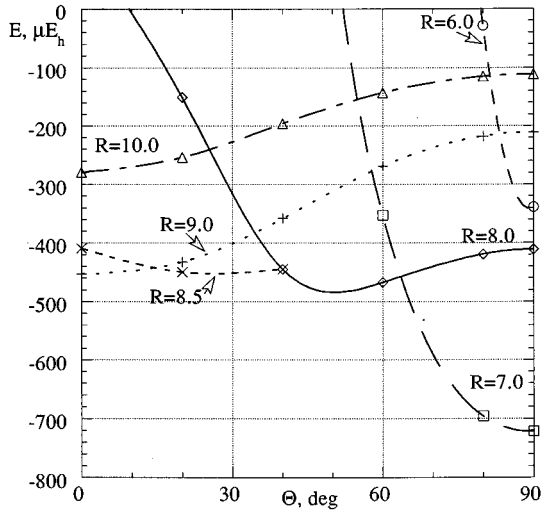

FIG. 1. The PES of the Ar–CO_2 cluster evaluated at the MP2/Sdf level.

TABLE II. MP4/Sdf(b-ext) calculations of interaction energy of Ar–CO_2 in μE_h.

R	Θ	ΔE^{SCF}	$\Delta E^{(2)}$	$\Delta E^{(3)}$	$\Delta E^{(4)}$	ΔE^{MP4}
6.53	90.0	654.3	−1545.3	265.3	−330.8	−956.6
7.0	90.0	245.6	−1028.1	178.3	−224.4	−828.7
8.0	90.0	21.5	−454.8	82.4	−101.9	−452.8
9.0	90.0	−5.63	−219.3	41.6	−49.5	−232.7
9.0	0.0	185.4	−682.8	142.6	−176.8	−531.6
9.45	0.0	63.9	−476.0	100.9	−127.6	−438.8
12.0	0.0	−5.11	−85.6	19.8	−25.2	−96.2

TABLE III. Interaction energy components for the Ar–CO_2 complex in the Sdf basis set (frozen-core calculations; R in a_0; energies in μH).

Θ	$\epsilon_{es}^{(10)}$	ϵ_{exch}^{HL}	ΔE^{HL}	$\epsilon_{ind,r}^{(20)}$	ΔE_{def}^{SCF}	$\epsilon_{disp}^{(20)}$	$\epsilon_{es,r}^{(12)}$	$\Delta E_{exch}^{(2)}$
				$R=5.0$				
0.0	−346 600.	1 019 200.	672 600.	−917.020	−175 250.	−72 619.	−8 744.2	47 801.
20.	−236 410.	678 180.	442 030	−584 220.	−105 460.	−55 614.	−5 884.7	27 082.
40.	−86 579.	243 120.	156 540.	−184 460.	−27 668.	−29 013.	−2 997.8	16 856.
60.	−24 231.	70 115.	45 884.	−44 899.	−5 681.9	−14 195.	−1 860.7	7 834.2
80.	−8 071.3	25 977.	17 906	−14 296.	−2 598.4	−8 820.0	−1 369.3	4 707.8
90.	−6 624.8	22 033.	15 408	−11 766.	−2 425.8	−8 251.5	−1 308.6	4 384.5
				$R=6.0$				
0.0	−47 733.	145 880	98 148.	−84 685	−14 717.	−20 007.	−3 677.9	14 585.
20.	−33 358.	100 780.	67 423.	−56 998.	−9 794.4	−15 895.	−2 651.7	10 573.
40.	−12 893.	38 510.	25 616.	−20 149.	−3 204.6	−9 032.3	−1 249.2	4 830.4
60.	−3 661.9	11 233.	7 670.8	−5 301.5	−778.6	−4 702.1	−522.0	1 877.3
80	−1 136.0	3 831.1	2 695.1	−1 677.5	−373.1	−3 003.8	−258.4	911.5
90.	−907.3	3 156.4	2 249.1	−1 369.4	−353.8	−2 819.3	−230.1	815.1
				$R=7.0$				
.0	−5 952.6	19 507.3	13 554.8	−7 437.0	−1 505.9	−5 901.4	−891.3	3 270.2
20.	−4 293.3	13 914.0	9 620.7	−5 313.9	−1 071.9	−4 872.4	−665.8	2 422.7
40.	−1 766.4	5 649.8	3 883.4	−2 126.5	−406.9	−2 993.8	−317.1	1 104.0
60.	−517.2	1 685.8	1 168.6	−616.9	−116.6	−1 681.9	−118.8	396.0
80.	−153.0	535.2	382.2	−210.7	−68.4	−1 125.3	−47.0	162.6
90.	−119.2	427.5	308.3	−175.4	−67.1	−1 062.5	−39.3	139.3
				$R=8.0$				
0.	−710.9	2 504.0	1 793.1	−688.8	−188.1	−1 936.0	−176.4	624.3
20.	−529.0	1 837.2	1 308.2	−519.6	−141.1	−1 652.5	−137.4	472.4
40.	−232.2	789.3	557.1	−233.2	−60.3	−1 093.6	−68.3	220.3
60.	−71.6	241.3	169.7	−77.0	−21.6	−665.9	−25.8	76.3
80.	−21.0	71.8	50.8	−32.1	−16.6	−471.4	−9.5	27.4
90.	−16.0	55.5	39.5	−28.2	−16.8	−448.8	−7.8	22.6
				$R=8.5$				
0.0	−244.7	887.0	642.3	−221.2	−74.5	−1 163.4	−77.0	263.5
20.	−185.0	659.3	474.4	−171.4	−57.1	−1 006.8	−61.3	201.1
40.	−84.2	290.7	206.6	−81.6	−26.0	−689.1	−31.5	95.3
				$R=9.0$				
0.0	−84.8	311.9	227.1	−76.8	−33.2	−722.9	−34.2	109.9
20.	−64.9	234.8	169.9	−61.0	−25.8	−633.1	−27.8	84.4
40.	−30.6	106.1	75.5	−30.5	−12.5	−446.8	−14.9	40.6
60.	−10.3	33.2	22.8	−11.8	−5.6	−293.6	−6.4	13.7
80.	−3.5	9.3	5.8	−6.9	−5.2	−219.8	−3.0	4.4
90.	−2.8	6.9	4.1	−6.6	−5.4	211.0	−2.6	3.5
				$R=9.5$				
0.0	−29.8	108.8	79.0	−30.0	−16.8	−464.2	−15.9	45.6
				$R=10.0$				
0.0	−10.8	37.6	26.7	−13.6	−9.6	−307.7	−8.1	19.0
20.	−8.4	29.1	20.7	−11.0	−7.6	−274.9	−6.8	14.7
40.	−4.3	13.8	9.5	−5.7	−3.9	−201.6	−4.3	7.2
60.	−1.8	4.4	2.6	−2.6	−2.0	−143.6	−2.5	2.2
80.	−1.0	1.1	0.1	−2.2	−2.0	−113.2	−1.5	0.6
90.	0.9	0.8	−0.1	−2.2	−2.1	−109.4	−1.3	0.5

C. Convergence of S-MPPT and basis set effects

Convergence of MPPT through the fourth order is shown in Table II. One can see that the major repulsive contribution is included in the SCF interaction energy. The dominant attractive contribution is encompassed in the second order $\Delta E^{(2)}$. The $\Delta E^{(3)}$ and $\Delta E^{(4)}$ corrections are smaller but important from a quantitative point of view. The pattern of convergence for both the T-shaped and collinear forms, and for different R, is similar. Namely, $\Delta E^{(3)}$ is repulsive and deteriorates the ΔE^{MP2} approximation; $\Delta E^{(4)}$ is attractive and somewhat larger in magnitude than $\Delta E^{(3)}$. It is also worthwhile to note that higher order correlation effects, which were found important in describing PESs of Ar interacting with rodlike molecules with multiple bonds,[35,36] are not affecting the shape of the surface in any major way in the present case.

Saturation of a basis set is another problem. It is expected that the MP4 level calculations using Sdf basis sets augmented with bond functions yield highly accurate results which are accurate to within ±5% in the neighborhood of the global minimum. The lowering of total interaction energy acquired by extending the basis set from Sdf to $Sdf(b\text{-ext})$ amounts to about 20% which is typical for Ar-molecule complexes.[16]

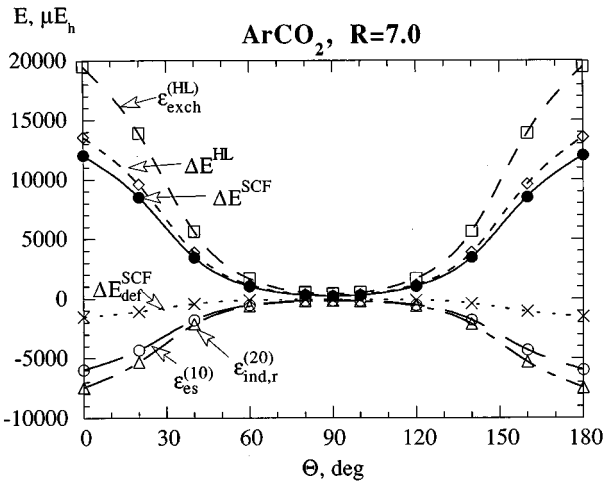

FIG. 2. The Θ dependence of the SCF components of interaction energy at $R=7.0\ a_0$ (Sdf basis set).

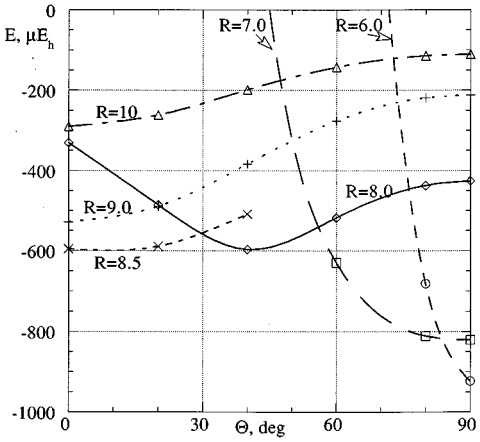

FIG. 4. The PES of the Ar–CO_2 cluster constructed as a sum of ΔE^{SCF} interaction energy and the dispersion $\epsilon_{\mathrm{disp}}^{(20)}$ energy from the Sdf calculations.

The basis set effects on the components of the interaction energy are displayed in Table IV. The comparison of three basis sets reveals fairly monotonic changes in the energy components with the basis set extension. The improvement of basis set has the strongest effect on the dispersion energy and it is chiefly responsible for the overall lowering of total interaction energy in our best basis set $Sdf(b\text{-ext})$. Some variations can be noticed in the electrostatic-correlation term, $\epsilon_{\mathrm{es},r}^{(12)}$, in accord with our previous conclusion that bond functions tend to deteriorate this component. However, in the particular case of Ar–CO_2, this term is very small and thus its variations may be safely neglected.

D. Nonadditive effects in the Ar_2CO_2 cluster

Three-body contributions to the interaction energy were shown to be very important in van der Waals clusters involving the Ar dimer bound to a chromophore.[27,37,38] In particular, the van der Waals infrared frequencies were found to differ from those predicted using the pairwise additivity assumption. The existing *ab initio* and experimental literature on these systems emphasizes the anisotropy of the three-body interactions as a chief factor affecting the shapes of the PESs of these clusters.[23–25,37,38]

We examined the three-body interaction and its perturbation components in two forms of the Ar_2CO_2 cluster shown in Fig. 5; (i) the form related to the T configuration of the $ArCO_2$ dimer and (ii) the form related to the L configuration of the same dimer. Hereafter these two structures are referred to as T-trimer and L-trimer, respectively. Both geometries were so chosen as to (approximately) minimize all two-body interactions in the trimer. The numerical results are shown in Table V.

First, we should notice that for both geometries the total nonadditive effect evaluated through the third order, ΔE^{MP3}, is repulsive and dominated by the three-body $\Delta E^{(3)}$ component. The $\Delta E^{(3)}$ nonadditivity is determined by the repulsive $\epsilon_{\mathrm{disp}}^{(30)}$ term. Due to additivity of $\epsilon_{\mathrm{disp}}^{(20)}$ and $\epsilon_{\mathrm{es},r}^{(12)}$ the nonadditiv-

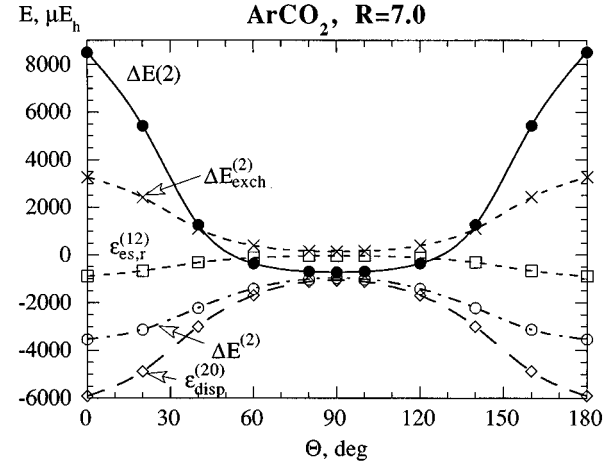

FIG. 3. The Θ dependence of the correlated components of interaction energy at $R=7.0\ a_0$ (Sdf basis set).

TABLE IV. Energy characteristics (in μE_{h}) of the configurations T and L of Ar–CO_2 (frozen-core approximation).

	Ar–CO_2 T			Ar–CO_2 L		
	S	Sdf	$Sdf(b\text{-ext})$	S	Sdf	$Sdf(b\text{-ext})$
	($R=7.0$, $\Theta=90.0°$)			($R=9.0$, $\Theta=0.0$)		
ΔE^{SCF}	253.6	241.2	245.6	186.1	194.0	185.4
$\Delta E^{(2)}$	−795.7	−962.5	−1028.1	−584.7	−647.2	−682.8
ΔE^{MP2}	−542.1	−721.3	−782.5	−398.7	−453.2	−497.4
ΔE^{MP4}	⋯	−757.5	−828.7	⋯	−482.6	−531.6
$\epsilon_{\mathrm{exch}}^{\mathrm{HL}}$	429.6	427.5	427.9	309.2	311.9	310.8
$\epsilon_{\mathrm{es}}^{(10)}$	−116.5	−119.2	−113.7	−90.3	−84.8	−90.8
$\Delta E_{\mathrm{def}}^{\mathrm{SCF}}$	−59.4	−67.1	−68.6	−32.9	−33.2	−34.6
$\epsilon_{\mathrm{ind},r}^{(20)}$	−168.5	−175.4	−176.1	−77.4	−76.8	−78.6
$\epsilon_{\mathrm{es},r}^{(12)}$	−37.8	−39.3	−54.4	−38.3	−34.2	−37.8
$\epsilon_{\mathrm{disp}}^{(20)}$	−891.6	−1062.5	−1111.3	−650.4	−722.9	−756.7
$\Delta E_{\mathrm{exch}}^{(2)}$	133.7	139.3	137.6	104.0	109.9	111.7
$\Delta E^{\mathrm{SCF}}+\epsilon_{\mathrm{disp}}^{(20)}$	−638.0	−821.2	−865.7	−464.3	−528.9	−571.3

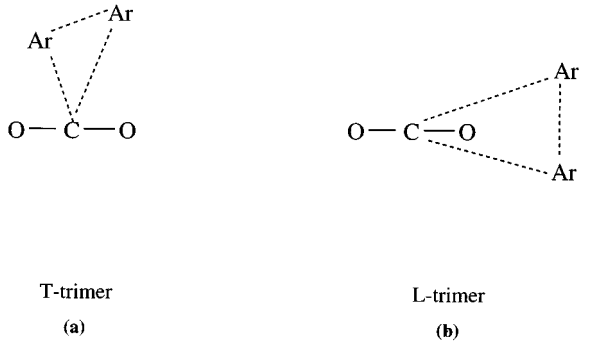

FIG. 5. Two configurations of the Ar_2CO_2 cluster considered in this work. (a) R(Ar–Ar)=7.1 a_0, R(C–Ar)=7.0 a_0; (b) R(Ar–Ar)=7.1 a_0, R(C–Ar) =9.0 a_0.

ity of $\Delta E^{(2)}$ is of secondary importance; it is small and repulsive for both geometries. The most important difference between the L- and T-trimers comes from the ΔE^{SCF} nonadditivity, which is negligibly repulsive for the T-trimer, but quite large and attractive for the L-trimer. Furthermore, as shown in Table V, the ΔE^{SCF} nonadditivity practically follows the behavior of the three-body HL-exchange effect ($\epsilon^{\mathrm{HL}}_{\mathrm{exch}}$). The three-body SCF-deformation term ($\Delta E^{\mathrm{SCF}}_{\mathrm{def}}$), on the other hand, is very similar for both geometries and very small compared to the total nonadditivity ΔE^{MP3}.

The sources of anisotropy of the $\epsilon^{\mathrm{HL}}_{\mathrm{exch}}$ nonadditivity in a variety of van der Waals clusters have been studied extensively for some time.[17,25,39,40] It is known that the $\epsilon^{\mathrm{HL}}_{\mathrm{exch}}$ term can be dissected into two contributions; (i) originating from the single exchanges within pairs of subsystem in a trimer (SE), and (ii) originating from the triple exchanges arising among all the monomers in the trimer (TE).[25,39,40] The SE effect creates the so called exchange-quadrupole moment on the Ar_2 subunit.[37,40] This exchange-quadrupole can then interact with the permanent quadrupole moment of the CO_2 molecule. CO_2 has a permanent quadrupole moment which is negative. When two negative quadrupoles interact so that their centers are the closest (as in the T-trimer) the interaction is repulsive. When the end of one quadrupole faces the center of the other (as in the L-trimer) the interaction is attractive. This qualitatively explains why the exchange nonadditivity is positive in the T and negative in the L-trimers.

The remaining TE part of the $\epsilon^{\mathrm{HL}}_{\mathrm{exch}}$ nonadditivity has a different orientation dependence, and should be included if qualitative details are needed.[16,25,39] The analytical modeling of this term was discussed in Ref. 39.

Overall the HL-exchange nonadditivity cancels a large portion of the three-body dispersion effect for the L-trimer and reinforces it for the T-trimer.

TABLE V. Energy decomposition (in μE_{h}) of the two-body and three-body terms for two configurations of the Ar_2CO_2 cluster in *S* basis set (all electron calculations).

	T-configuration			L-configuration		
	CO_2–Ar	Ar–Ar	Ar_2–CO_2	CO_2–Ar	Ar–Ar	Ar_2–CO_2
ΔE^{SCF}	252.9	429.5	2.2	127.0	430.1	−9.6
$\Delta E^{(2)}$	−801.3	−625.1	3.1	−498.2	−622.4	5.7
$\Delta E^{(3)}$	166.4	118.0	22.7	144.4	117.9	15.3
ΔE^{MP2}	−548.4	−195.6	ΔE^{MP3}:27.9	−371.2	−192.3	ΔE^{MP3}:11.5
$\epsilon^{\mathrm{HL}}_{\mathrm{exch}}$	429.4	644.3	0.8	212.0	644.0	−10.7
$\epsilon^{(10)}_{\mathrm{es}}$	−116.6	−188.4	0	−61.8	−187.7	0
$\Delta E^{\mathrm{SCF}}_{\mathrm{def}}$	−59.9	−26.4	1.4	−23.3	−26.2	1.14
$\epsilon^{(20)}_{\mathrm{ind},r}$	−168.9	−233.3	−3.5	−55.9	−232.7	2.8
$\epsilon^{(12)}_{\mathrm{es},r}$	−39.1	−41.2	0	−29.3	−41.4	0
$\epsilon^{(20)}_{\mathrm{disp}}$	−899.1	−731.2	$\epsilon^{(30)}_{\mathrm{disp}}$:23.3	−544.2	−727.9	$\epsilon^{(30)}_{\mathrm{disp}}$:16.4
$\Delta E^{(2)}_{\mathrm{exch}}$	136.9	147.3	3.1	75.3	146.9	5.7
$\epsilon^{(21)}_{\mathrm{disp}}$	176.8	122.0	0	121.5	121.9	0

E. Analytical two-body potential of Ar–CO_2

The PES of the Ar–CO_2 complex was presented as sum of the short-range repulsive term (V_{sr}), the dispersion energy term (V_{disp}) and the induction energy term (V_{ind}),

$$V = V_{\mathrm{sr}} + V_{\mathrm{disp}} + V_{\mathrm{ind}}. \tag{6}$$

According to Buckingham, Fowler, and Hutson,[41] for the atom interacting with a rodlike molecule, V_{sr} may be conveniently represented using the independent angular expansions of a reference distance (R_{ref}) and the exponent (β) as follows:

$$V_{\mathrm{sr}}(R,\Theta) = A\ \exp\{-\beta(\Theta)[R - R_{\mathrm{ref}}(\Theta)]\}, \tag{7}$$

where

$$R_{\mathrm{ref}}(\Theta) = \sum_L R_{\mathrm{ref},L} P_L(\cos\Theta),$$

$$\beta(\Theta) = \sum_L \beta_L P_L(\cos\Theta).$$

The dispersion part of PES was represented using the following damped expansion:

$$V_{\mathrm{disp}} = -\sum_{n=6}^{\mathrm{even}} \sum_{L=0}^{n-4} \frac{D_n(\beta,R) C^{\mathrm{disp}}_{n,L} P_L(\cos\Theta)}{R^n}, \tag{8}$$

where

$$D_n(\beta,R) = 1 - \exp(-\beta R) \sum_{k=0}^{n} \frac{[\beta(\Theta)R]^k}{k!},$$

are the damping functions of Tang and Toennies,[42] and $P_L(\cos\Theta)$ are Legendre polynomials.

The induction part of the PES was represented using the following expression:[43]

$$V_{\mathrm{ind}} = -\sum_{n=8}^{\mathrm{even}} \sum_{L=0}^{n-4} \frac{C^{\mathrm{ind}}_{n,L} P_L(\cos\Theta)}{R^n} = V_{\mathrm{ind}}(\mathrm{moments}). \tag{9}$$

In the case of a centrosymmetric molecule interacting with Ar, it is sufficient to consider only the n-even terms in Eqs. (8) and (9). In the Eqs. (7)–(9) A, β_L, $R_{\mathrm{ref},L}$, $C^{\mathrm{disp}}_{n,L}$ were treated as adjustable parameters. The attempts to treat $C^{\mathrm{ind}}_{n,L}$ as adjustable parameters have led to unphysical leading terms. Therefore, $C^{\mathrm{ind}}_{n,L}$ were evaluated from the *ab initio* de-

rived multipole moments and polarizabilities of the monomers[43] and hence the induction term in our analytical potential was denoted V_{ind}(moments).

The V_{disp} term of Eq. (8) was fitted to the $\epsilon_{\mathrm{disp}}^{(20)}$ values from Table III. V_{sr} was fitted to the sum of the Heitler–London energy, ΔE^{HL}, the second-order exchange term, $\Delta E_{\mathrm{exch}}^{(2)}$, the electrostatic correlation term, $\epsilon_{\mathrm{es},r}^{(12)}$, and the exchange and overlap parts of $\Delta E_{\mathrm{def}}^{\mathrm{SCF}}$. The total $\Delta E_{\mathrm{def}}^{\mathrm{SCF}}$ component includes the R^{-n} long-range induction terms in addition to the exchange and overlap contributions. In order to remove the R^{-n} part, the V_{ind}(moments) term was subtracted from it. V_{sr} was thus fitted to the following sum:

$$\epsilon_{\mathrm{exch}}^{\mathrm{HL}}+\epsilon_{\mathrm{es}}^{(10)}+\Delta E_{\mathrm{exch}}^{(2)}+\epsilon_{\mathrm{es},r}^{(12)}+[\Delta E_{\mathrm{def}}^{\mathrm{SCF}}-V_{\mathrm{ind}}(\mathrm{moments})].$$

It should be mentioned at this point that the induction energy is perhaps the most difficult to model analytically because it often couples very strongly with the exchange effects [this coupling is reflected by the disparities between the values of $\epsilon_{\mathrm{ind},r}^{(20)}$ and $\Delta E_{\mathrm{def}}^{\mathrm{SCF}}$, especially in the repulsive range of the PES, see Table III]. For this reason it is more justified to fit to the $\Delta E_{\mathrm{def}}^{\mathrm{SCF}}$ values than to the $\epsilon_{\mathrm{ind},r}^{(20)}$ values.

The fit of V_{disp} was prepared in three stages. First a general analytical form was prepared by fitting to the interaction energy data obtained using the *Sdf* basis set (Table III). In the second step the dispersion energies at the selected points were scaled to reproduce the MP4/*Sdf* values from Table I in the following way:

$$V_{\mathrm{disp}}(\mathrm{MP4}/Sdf)=V(\mathrm{MP4}/Sdf)-V_{\mathrm{sr}}(\mathrm{MP2}/Sdf)-V_{\mathrm{ind}}(\mathrm{moments}).$$

The final step involved scaling of the V_{disp} (MP4/*Sdf*) values to match the total interaction energies at the MP4/*Sdf*(*b*-ext) level,

$$V=V_{\mathrm{sr}}(\mathrm{MP2}/Sdf)+V_{\mathrm{ind}}(\mathrm{moments})+f_b\cdot V_{\mathrm{disp}}(\mathrm{MP4}/Sdf),$$

where the scaling factors f_b were determined from

$$f_b=\{\Delta E[\mathrm{MP4}/Sdf(b\text{-ext})]-V_{\mathrm{sr}}(\mathrm{MP2}/Sdf)-V_{\mathrm{ind}}(\mathrm{moments})\}/V_{\mathrm{disp}}(\mathrm{MP4}/Sdf)$$

at the selected points along the $\Theta=0°$ and 90° cuts (see Table II).

The dispersion coefficients were forced to be positive and constraints were placed on the values of V and dV/dR (especially at the global minimum and for the linear configuration). The obtained parameters of the analytical potential are displayed in Table VI along with the comparison of the well depth and saddle point data.

TABLE VI. Obtained parameters of the analytical two-body potential energy surface of Ar–CO_2 [see Eqs. (6)–(9), all values in a.u.; numbers in parentheses denote powers of ten].

V_{sr}	V_{ind} (moments)[a,b]	V_{disp}
$A=4.358\ 89(1)$	$C_{8,0}^{\mathrm{ind}}=2.029\ 45(2)$	$C_{6,0}^{\mathrm{disp}}=1.861\ 78(2)$
$R_{\mathrm{ref},0}=1.496\ 81$	$C_{8,2}^{\mathrm{ind}}=2.319\ 37(2)$	$C_{6,2}^{\mathrm{disp}}=1.065\ 32(2)$
$R_{\mathrm{ref},2}=1.359\ 45$	$C_{8,4}^{\mathrm{ind}}=1.739\ 53(2)$	$C_{8,0}^{\mathrm{disp}}=0.0$
$R_{\mathrm{ref},4}=1.037\ 11(-1)$	$C_{10,0}^{\mathrm{ind}}=4.257\ 40(3)$	$C_{8,2}^{\mathrm{disp}}=0.0$
$R_{\mathrm{ref},6}=-2.320\ 85(-1)$	$C_{10,2}^{\mathrm{ind}}=4.359\ 70(3)$	$C_{8,4}^{\mathrm{disp}}=0.0$
$R_{\mathrm{ref},8}=1.741\ 00(-1)$	$C_{10,4}^{\mathrm{ind}}=2.356\ 01(3)$	$C_{10,0}^{\mathrm{disp}}=2.932\ 58(5)$
$\beta_0=1.857\ 82$	$C_{10,6}^{\mathrm{ind}}=6.869\ 52$	$C_{10,2}^{\mathrm{disp}}=5.286\ 39(5)$
$\beta_2=2.093\ 64(-2)$		$C_{10,4}^{\mathrm{disp}}=0.0$
$\beta_4=1.016\ 25(-1)$		$C_{10,6}^{\mathrm{disp}}=0.0$
$\beta_6=-9.647\ 34(-2)$		
$\beta_8=6.985\ 41(-2)$		
Θ:	90°	0°
σ_0	5.800	8.089
R_m	6.566	8.897
V_m	956.72	515.11

[a]The *ab initio* values of monomer properties were as follows: the dipole and quadrupole polarizabilities of Ar were 9.57 a.u. and 43.02 a.u., respectively; the quadrupole and hexadecapole moments of CO_2 were -3.76 a.u. and -0.06 a.u., respectively.

[b]The dispersion coefficients were further scaled by 1.012 in order to better represent the MP4/*Sdf*(*b*-ext) values.

IV. SUMMARY AND CONCLUSIONS

The global minimum of the Ar–CO_2 intermolecular potential occurs for the T-shaped geometry with $\Theta=90°$ and at $R=6.5\ a_0$. The best estimate of D_e is 957 μE_{h} obtained with the *Sdf*(*b*-ext) basis set at the MP4 level of theory. The estimate of the minimum depth is expected to be accurate within $\pm 5\%$. The potential well is somewhat deeper than that of Bohac *et al.* ($R_e=6.5\ a_0$ and $D_e=894\ \mu E_{\mathrm{h}}$).[7] Our PES reveals an extremely flat region near the linear geometry of this cluster. The lowest point at this plateau, probably a saddle point, is found for $\Theta=0°$ and $R=9.0\ a_0$ and stabilized by $\sim 533\ \mu E_{\mathrm{h}}$. The latter result is substantially larger than the empirical estimate of 260 μE_{h} of Bohac *et al.*[7] It is important to point out that the spectroscopic data used in the fit of Bohac *et al.*[7] are not sensitive to the regions of the potential far from the minimum. Therefore, those regions of the empirical potential may be more seriously in error.

It is interesting to analyse the origin of the minima on the Ar–CO_2 surface. The origin of the global minimum is clear; it occurs for the configuration which corresponds to the local depletion of electron density and the resulting local minimum in the HL-exchange repulsion. At the same time, owing to a triangular arrangement which brings Ar close to both C and O atoms, the dispersion stabilization is relatively strong. The origin of stabilization of the collinear areas is more complex. Neither exchange nor induction play a major role. Indeed, the ratio def/disp which we customarily use to measure the relative importance of the induction term[16] comes out close to an insignificant 3% for the linear arrangement. As to the exchange effects, within the CO_2 molecule there are no visible lone pairs on the O atoms, thus no relative reduction of exchange-repulsion on the OCO axis occurs. The only meaningful factor which minimizes the interaction energy in this area is the dispersion term. Since the dispersion energy is known to be less anisotropic than the exchange and induction contributions, the PES has a pronounced plateau in the linear region.

The three-body interactions in the Ar_2CO_2 cluster were examined for the two configurations related to the T and L configurations of the dimer $ArCO_2$. The qualitative features of the anisotropy of these interactions were found to be con-

sistent with the exchange-quadrupole model of Cooper and Hutson.[37]

Note added in proof. The direct spectroscopic observation of three-body effects in Ar_2CO_2 has recently been reported by Sperhac, Weida, and Nesbitt (Ref. 44).

ACKNOWLEDGMENTS

The support by the National Science Foundation is acknowledged by M.M.S. and G.C. (Grant No. CHE-9215082) and by C.J.J. (Grant No. CHE-9210790). The support by the Polish Committee for Scientific Research KBN is acknowledged by J.S. (Grant No. BST/12-502-20/95) and by G.C. (Grant No. BST/12-501/III/502/23/95).

[1] S. Green and J. M. Hutson J. Chem. Phys. **100**, 891 (1994).
[2] G. A. Parker, R. L. Snow, and R. T. Pack, J. Chem. Phys. **64**, 1668 (1976).
[3] R. K. Preston and R. T. Pack, J. Chem. Phys. **66**, 2480 (1977).
[4] J. M. Steed, T. A. Dixon, and W. Klemperer, J. Chem. Phys. **79**, 4095 (1979).
[5] A. M. Hough and B. J. Howard, J. Chem. Soc. Faraday Trans. 2 **83**, 173 (1987).
[6] S. W. Sharpe, D. Reifschneider, C. Wittig, and R. A. Beaudet, J. Chem. Phys. **94**, 233 (1991).
[7] E. J. Bohac, M. D. Marshall, and R. E. Miller, J. Chem. Phys. **97**, 4890 (1992).
[8] C. F. Roche, A. Ernesti, J. M. Hutson, and A. S. Dickinson, J. Chem. Phys. **104**, 2156 (1996).
[9] K. Szalewicz and B. Jeziorski, Mol. Phys. **38**, 191 (1979).
[10] (a) S. Rybak, B. Jeziorski, and K. Szalewicz, J. Chem. Phys. **95**, 6576 (1991); (b) H. L. Williams, K. Szalewicz, B. Jeziorski, R. Moszyński, and S. Rybak, *ibid*. **98**, 1279 (1993).
[11] B. Jeziorski, R. Moszyński, and K. Szalewicz, Chem. Rev. **94**, 1887 (1994).
[12] G. Chałasiński and M. M. Szczęśniak, Mol. Phys. **63**, 205 (1988).
[13] S. M. Cybulski, G. Chałasiński, and R. Moszyński, J. Chem. Phys. **92**, 4357 (1990).
[14] S. M. Cybulski and G. Chałasiński, Chem. Phys. Lett. **197**, 591 (1992).
[15] R. Moszyński, S. M. Cybulski, and G. Chałasiński, J. Chem. Phys. **100**, 4998 (1994).
[16] 5. G. Chałasiński and M. M. Szczęśniak, Chem. Rev. **94**, 1723 (1994).
[17] B. Jeziorski, M. Bulski, and L. Piela, Int. J. Quantum Chem. **10**, 281 (1976).
[18] M. Gutowski, G. Chałasiński, and J. van Duijneveldt-van de Rijdt, Int. J. Quantum Chem. **26**, 971 (1984).
[19] M. Gutowski and L. Piela, Mol. Phys. **64**, 943 (1988).
[20] S. M. Cybulski, J. Chem. Phys. **97**, 7545 (1992).
[21] R. Moszyński, S. Rybak, S. M. Cybulski, and G. Chałasiński, Chem. Phys. Lett. **166**, 609 (1990).
[22] B. M. Axilrod and E. Teller, J. Chem. Phys. **11**, 299 (1943).
[23] M. M. Szczęśniak and G. Chałasiński, J. Mol. Struct. (Theochem) **261**, 37 (1992).
[24] M. J. Elrod, R. J. Saykally, Chem. Rev. **94**, 1975 (1994).
[25] S. M. Cybulski, M. M. Szczęśniak, and G. Chałasiński, J. Chem. Phys. **101**, 10 708 (1994); M. M. Szczęśniak, G. Chałasiński, and P. Piecuch, *ibid*. **99**, 6732 (1993).
[26] M. Gutowski and G. Chałasiński, J. Chem. Phys. **98**, 5540 (1993); G. Chałasiński and M. Gutowski, Chem. Rev. **88**, 943 (1988).
[27] J. H. van Lenthe, J. G. C. M. van Duijneveldt-van de Rijdt, and F. B. van Duijneveldt, Adv. Chem. Phys. **69**, 521 (1987).
[28] S. F. Boys and F. Bernardi, Mol. Phys. **19**, 553 (1970).
[29] M. J. Frisch, G. W. Trucks, M. Head-Gordon, P. M. W. Gill, M. W. Wong, J. B. Foresman, B. G. Johnson, H. B. Schlegel, M. A. Robb, E. S. Replogle, R. Gomperts, J. L. Andres, K. Raghavachari, J. S. Binkley, C. Gonzalez, R. L. Martin, D. J. Fox, D. J. Defrees, J. Baker, J. J. P. Stewart, and J. A. Pople, GAUSSIAN 92, Gaussian, Inc., Pittsburgh, Pennsylvania, 1992.
[30] S. M. Cybulski, TRURL94 package, Rochester, Michigan, 1994.
[31] A. J. Sadlej, Coll. Czech. Chem. Commun. **53**, 1995 (1988).
[32] G. Chałasiński, D. J. Funk, J. Simons, and W. H. Breckenridge, J. Chem. Phys. **87**, 3569 (1987). (Regrettably there are two misprints in this paper; the exponents of *d*-symmetry orbitals should be 0.84 and 0.174, and that of *f*-symmetry orbital 0.23.)
[33] (a) F-M. Tao and Y-K. Pan, J. Chem. Phys. **97**, 4989 (1992); (b) F-M. Tao, *ibid*. **98**, 3049 (1992).
[34] R. F. W. Bader and T. A. Keith, J. Chem. Phys. **99**, 3683 (1993).
[35] R. Moszyński, P. E. S. Wormer, and A. van der Avoird, J. Chem. Phys. **102**, 8385 (1995).
[36] F.-M. Tao, S. Drucker, and W. Klemperer, J. Chem. Phys. **102**, 7289 (1995).
[37] A. R. Cooper and J. M. Hutson, J. Chem. Phys. **98**, 5337 (1993).
[38] M. A. Suhm and D. J. Nesbitt, Chem. Soc. Rev. **24**, 45 (1995).
[39] G. Chałasiński J. A. Rak, S. M. Cybulski, and M. M. Szczęśniak (in preparation).
[40] L. Jansen, Adv. Quantum Chem. **2**, 119 (1965).
[41] A. D. Buckingham, P. W. Fowler, and J. M. Hutson, Chem. Rev. **88**, 963 (1988).
[42] K. T. Tang and J. P. Toennies, J. Chem. Phys. **80**, 3726 (1984).
[43] P. E. S. Wormer, H. Hettema, and A. J. Thakkar, J. Chem. Phys. **98**, 7140 (1993).
[44] J. M. Sperhac, M. J. Weida, and D. J. Nesbitt, J. Chem. Phys. **104**, 2202 (1996).